A Low Power, Battery Operated Precision Portable Thermal Chamber with Double Thermoelectric Module

Anderson W. Spengler, Elnatan C. Ferreira, and J. A. Siqueira Dias

***Abstract*—**A low-power thermal chamber with a volume of only 2.5 liters capable of reaching temperatures over the -5ºC to 70ºC range was designed and constructed. Two small 12 V batteries are used as the power supply for the complete system. Thermoelectric modules were used as actuators since their size and performance characteristics allow the portability and precise temperature control. The PID control provided stability and errors better than normally found in expensive commercial thermal chambers, with maximum temperature error of ±0.2ºC with respect to the setpoint and with a fluctuation of ±0.1ºC.

***Keywords*—**Thermal chamber, Thermoelectric modules, Stacked Thermoelectric modules, Analog PID, Temperature control, H-Bridge Power Driver.

I. Introduction

COMMERCIALthermal chambers have a large volume, which makes them inappropriate for portable bench-top or field applications. The technology used in commercial thermal chambers employ compressors and radiators to cool down the chamber, requiring a lot of space and making them difficult to control with low steady-state temperature errors. To overcome these problems, this paper presents a technique where thermal electric modules (TEM) were used, making the equipment small and easier to control, resulting in a reduced size lightweight portable equipment that can be used in the field or in bench-top applications where precise temperature control are needed.

II. Design of the Thermal Chamber

The chamber size, insulation and materials are determinant in estimating the amount of power that will be required to cool or heat the chamber. The thermal chamber has the external dimensions of 300 mm x 240 mm x 120 mm and the internal space is 240 mm x 180 mm x 60 mm (approximately 2.6 l). The insulation is made of an elastomer foam with thermal conductivity of 0.037 W/(m.K) at 20ºC, and its thickness is only 30 mm.

To estimate the required power to cool the chamber, the AZTEC software [1] was used, and for the given dimensions and desired temperature, the program indicates that it is necessary 10.58 W, considering that an active internal load is dissipating 1W.

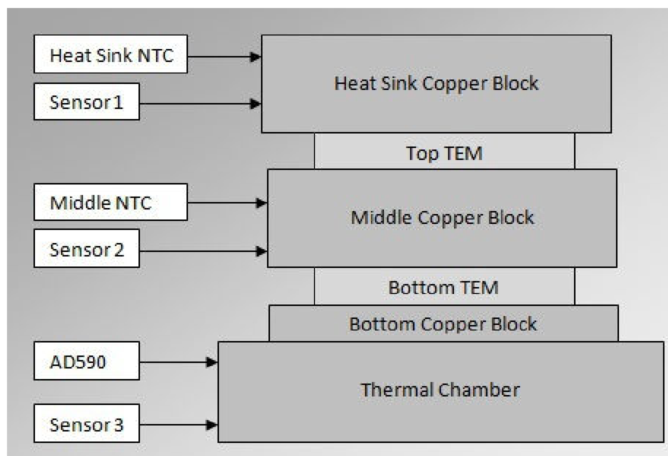

Fig.1 – Actuators assembling diagram.

An interesting feature of this design is that two TEMs are used in a series configuration, in order to reduce the temperature difference between the ceramic plates and, therefore, allow for higher heat transportation. The thermal chamber is built in two parts, which are united by a central element with two Teflon pieces in order to centralize the aluminum central parts. Fig.1 shows the block diagram of the structure, the position of TEMs, sensors and copper blocks.

Since a critical part of TEM is dissipating the transported heat and the generated heat in this transportation, it was necessary to use a heat sink to remove the heat from the hot side of the top TEM. According to reference [2], the used heat sink will be 15º C above room temperature for a 125W load. The final assembling of the thermal chamber is done by fastening into the inner piece the module composed by the TEMs, copper blocks, heat sink, sensors and insulator. After this, the internal fan (required to make the spacial distribution

Manuscript received October 9, 2007: Revised version received March 4, 2008.

Anderson Spengler is with the School of Electrical and Computer Engineering FEEC/UNICAMP, 400 Albert Einstein Ave, 13083-852 Campinas SP BRAZIL (e-mail: spengler@demic.fee.unicamp.br).

Elnatan C. Ferriera is with the School of Electrical and Computer Engineering FEEC/UNICAMP, 400 Albert Einstein Ave, 13083-852 Campinas SP BRAZIL (e-mail: elnatan@demic.fee.unicamp.br).

J. A. Siqueira Dias is with the School of Electrical and Computer Engineering FEEC/UNICAMP, 400 Albert Einstein Ave, 13083-852 Campinas SP BRAZIL (phone: +551935214901; fax: +551935214896, e-mail: siqueira@demic.fee.unicamp.br).

of the heat more uniform and equalize the internal temperature) and the heat sink are also fixed in the inner piece. A photograph of the constructed thermal chamber with the temperature control board on its top is shown in Fig.2.

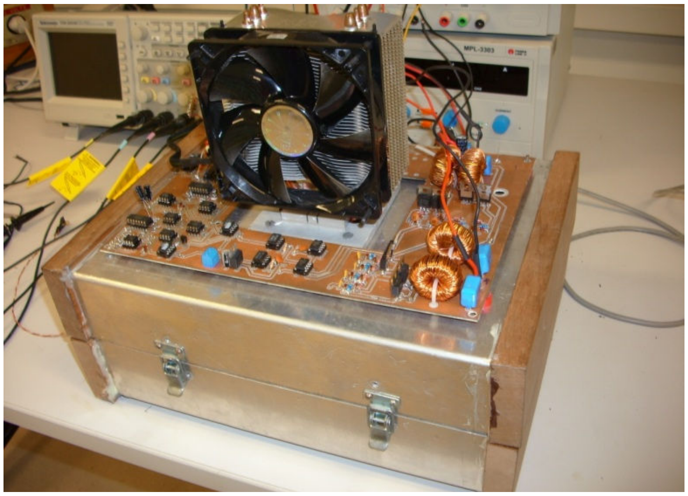

Fig.2 – Thermal chamber constructed.

III. Eletronics Circuits

The block diagram of the thermal chamber circuits is presented in Fig.3. The electronics circuits are used both to read the temperature (with digital integrated sensors) and to control the internal temperature by adequately driving the TEMs.

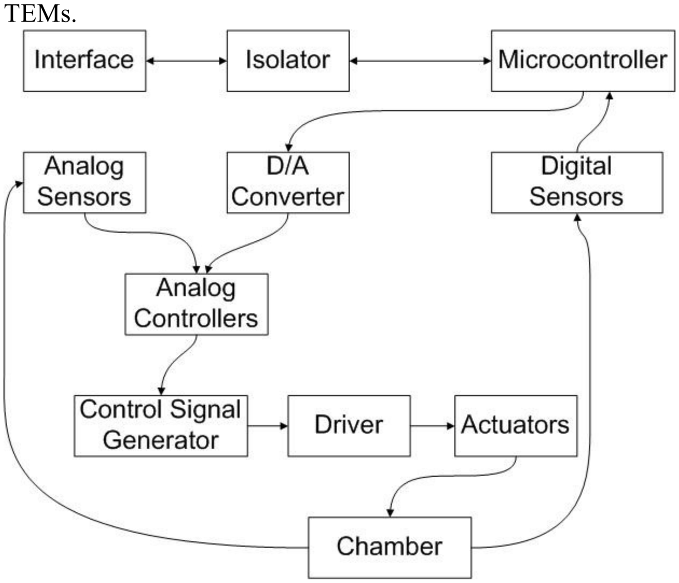

Fig.3 – Block diagram of the thermal chamber circuits.

The microcontroller (PIC16F872A) [3] communicates with the interface module through a transceiver which has a galvanic insulation, the ADM2483 [4]. The digital temperature sensors employed were implemented with the LM95071 [5], which is a very fast and high resolution (12 bits) integrated temperature transducer. To measure the relative humidity inside de thermal chamber it was used a SHT15 [6]. Although it has the capability of measuring temperature, it was used only as a humidity sensor since is very slow and would jeopardize the performance of the temperature control. The setpoint voltage of the PID controller for the bottom TEM is determined by the user, and is internally generated with a 12 bits D/A converter with SPI communication (TLV5616) [7].

The analogs sensors used are two 2.2 kΩ B57891M Series NTCs [8] and one AD590 [9]. The NTCs are fixed in the middle block and in the heat sink, since high precision is not required in these points. The AD590 is located inside the thermal chamber, where it is necessary a high accuracy in the temperature measurement. The three sensors signals are conditioned to present 32 mV/ºC, which is the same scale used in the D/A converter. In Fig.4 the schematic diagram used in the signal conditioning of the NTCs is shown.

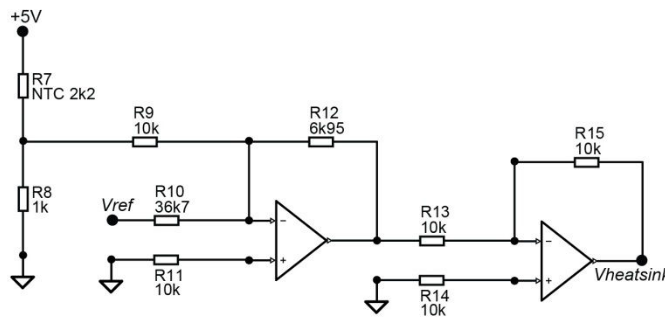

Fig.4 – NTC signal conditioning circuit.

The AD590 signal conditioning circuit is presented in Fig.5.

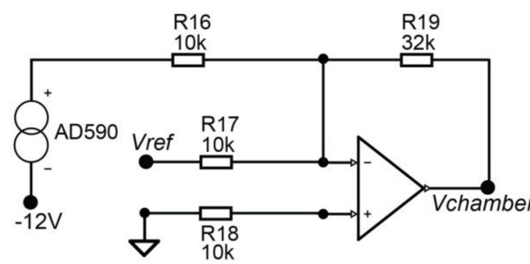

Fig.5 – Conditioning circuit for the AD590.

The setpoint of the PID controller of the bottom TEM is determined by the user, and it is defined by a signal that comes from the D/A converter. To optimize the operation of the top TEM, its temperature setpoint is automatically chosen by the circuitry, and given by the following equation:

$$v_{setpoint} = 0.8v_{chamber} + 0.2v_{heatsink} \quad (1)$$

where v_{chamb} is the voltage related to chamber temperature and v_{heatsi} is the voltage related to the heatsink temperature. This equation was obtained experimentally, measuring many TEM voltage configurations in order to obtain the highest cooling and heating efficiency.

The complete PID circuit of the bottom TEM is shown in Fig.6. The choice of using an analog PID controller following the format proposed in [10] was due the low cost and good performance results which can be obtained with this circuit, so it was not necessary to use a PID controller as describe in [11]. The PID parameters (proportional, integral and derivative gains) are adjusted individually (and separately), offering more flexibility to the system. The summing amplifier can introduce signal attenuations of each signal coming from the PID main block.

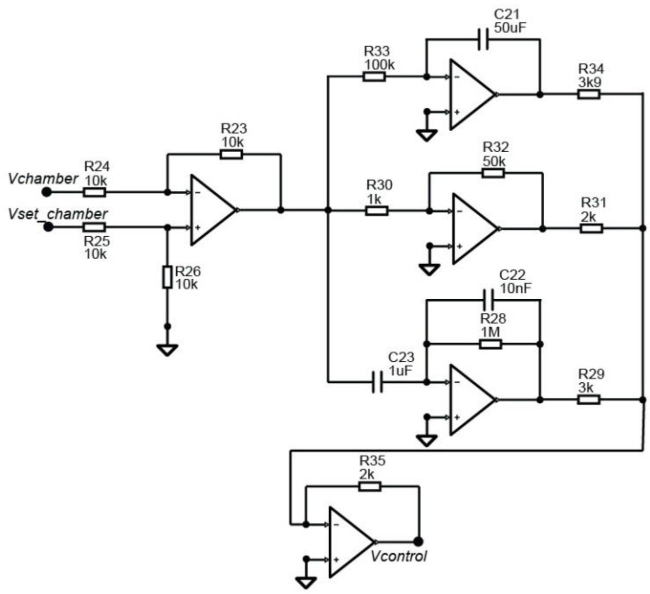

Fig.6 – PID circuit used for the bottom TEM control.

Due to the high current required by the CP14-127-045 TEMs [12], an H-bridge composed of MOSFET transistors driven by a PWM signal was used. To obtain the PWM signal, a conventional approach was adopted. A triangular wave with frequency $f_{PWM} = 5\ k$ is generated and compared to the PID output signal. The output of the comparator is the required PWM signal. The circuit of the triangular wave generator and the comparator is show in Fig.7.

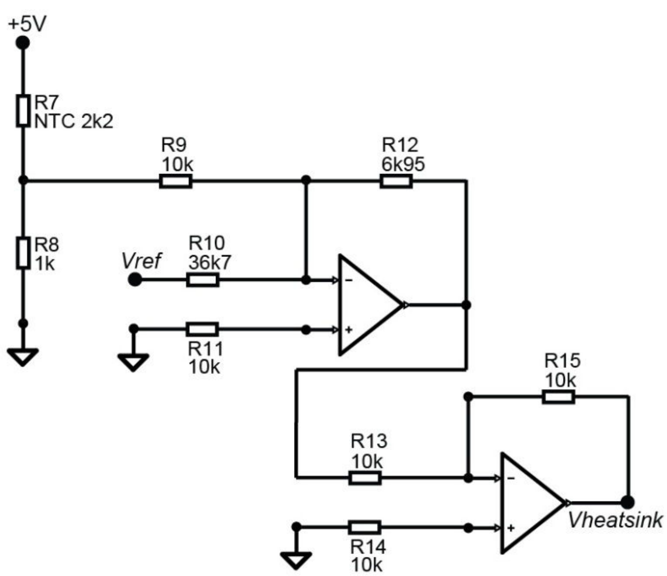

Fig.7 – Triangular wave generator and comparator circuits used for the TEMs controls.

To ensure that the ideal voltage limits were not exceeded in the PID controller output circuits, limiter circuits were added, as shown in Fig.8.

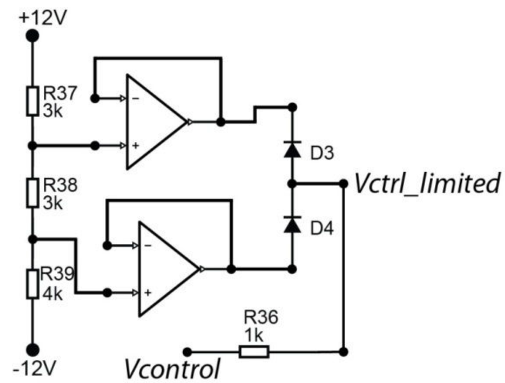

Fig.8 – Limiter circuit.

The PWM signal is sent to the H-bridge circuit through an optoisolator HCPL4503 [13], connected to two TC4428 [14] drivers, resulting in two complementary PWM signals outputs. To guarantee a continuous voltage level, LC filters are used in the output of the H-bridge.

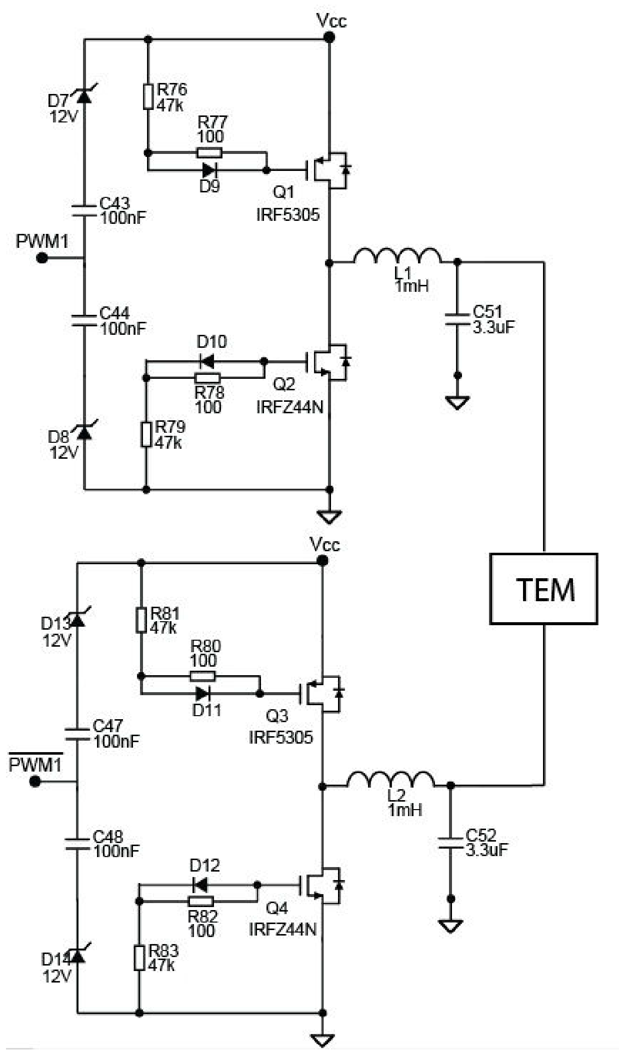

Fig.9 – PID circuit used for the bottom TEM control.

IV. User Interface

A user interface was implemented using Labview [22]. The objective of this interface is to provide a user friendly environment to the users of the thermal chamber. With this interface the user can operate the equipment and does not need to know the microcontroller commands, such as the communication protocol, desired chamber temperature command settings or the temperature and humidity readings commands.

The algorithm is very intuitive. The program starts with the communication initialization, so the software sends to the microcontroller the chamber temperature set point and begins the readings (stars with the temperatures and ends with the humidity readings). After a complete set of data acquisition, a correction of the values is made. This correction uses the calibration results to adjust the temperature values, and next the values are showed to the user. If the software recognizes a change in the set point value, it sends the new setpoint value. If not, a new round of data acquisition is performed. The block diagram of the software is shown in Fig. 10.

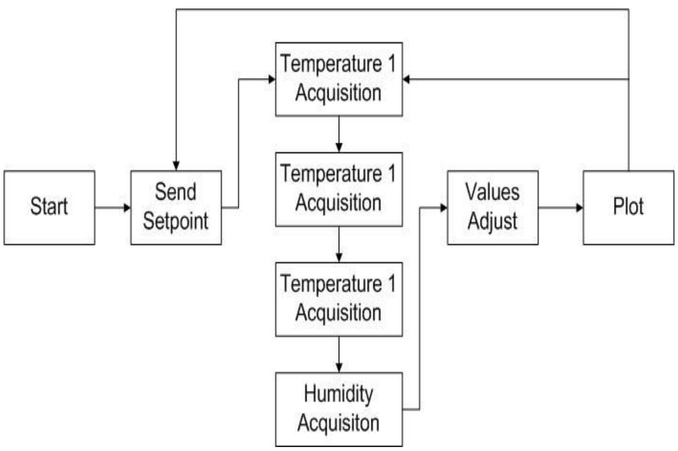

Fig.10 – Block diagram of the user interface software.

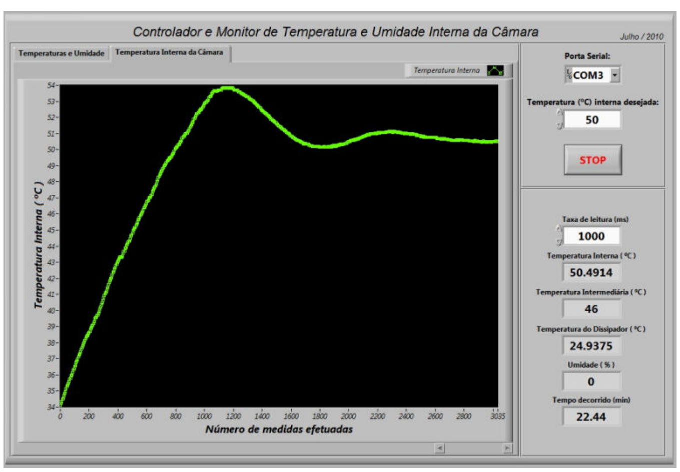

Fig.11 – Main window of the user interface.

The main window viewed by the user is presented in Fig.11. The graph shown is the behavior of the temperature inside the chamber. At the top right of the screen is possible to see the setup that the user must make, like the serial port used, the desired temperature and the time between readings.

At the bottom right it is possible to see the heatsink and intermediary temperatures as well as the instantaneous temperature and humidity inside the chamber.

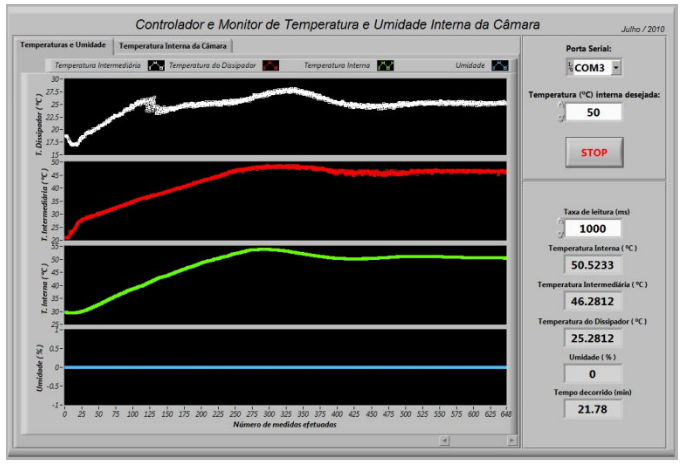

Fig.12 – Secondary window of the user interface.

Another window of the user interface is shown in Fig.12. In this window the user has the variation with time of the heat sink temperature, intermediary temperature, and the temperature and the humidity inside the chamber.

V. Experimental Results

The first test performed was to determine the minimum internal temperature that could be reached with the thermal chamber, driving the TEMs with a constant voltage source. The measured results are presented in Fig.13. The test starts with a nitrogen flux inside the chamber, with 13 V and 6 A on the top TEM and 5 V and 2.6 A on the bottom TEM. Although the relative humidity measured reaches -2%, it is not an error since sensor´s manufacturer [6] informs that negative values should be considered as zero. The nitrogen flow was turned off 150 minutes after the beginning of the test, and an increase of the humidity is observed.

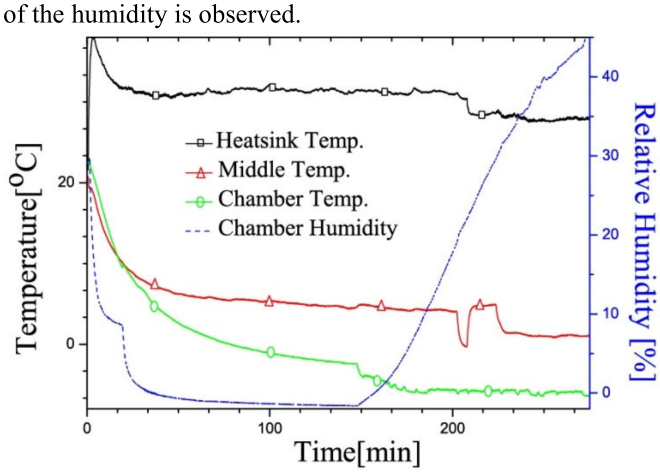

Fig.13 – Measurement result to obtain the lowest temperature in the chamber.

At the end of the measurement cycle, the following temperatures were observed: -6.4ºC inside the chamber, 1ºC in the intermediary block, and 27.8ºC at the heat sink. Using these values of measured temperatures and the graphs provided by [12], it was possible to estimate that the transported power by each of the TEMs modules as: 20 watts for the top TEM (which is well above the 11 watts calculated by the manufacturer´s software), and around 30 watts for the bottom TEM, which is in agreement with the 28.8W predicted by the software.

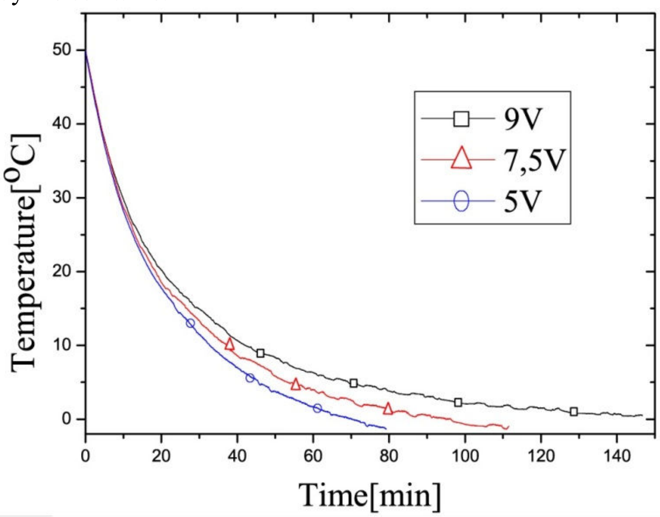

Fig.14 – Experimental results to view the system cooling behavior.

The difference observed in the top TEM is justified by the unavoidable heat leakage from the chamber and also due to the insulation between the heat and cold sides of the TEM.

Due to the system nonlinearity in the heating and cooling process, the PID tuning parameters were obtained experimentally. The optimal voltage for the bottom and top TEMs were also determined experimentally, after several experimental tests. These experimental tests consisted basically in changing the supply voltage of the thermoelectric modules and observing how the system responded. The measured results for cooling the system are presented in Fig.14. The top TEM was powered with 12 volts and the bottom TEM had its power supply voltage changed as shown in the graph.

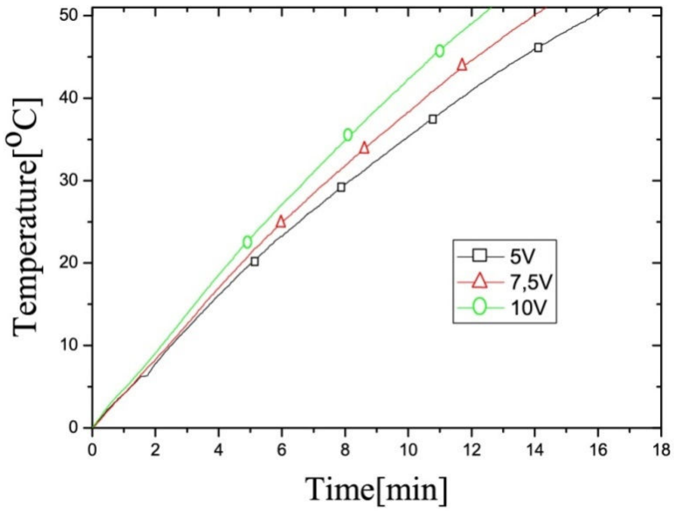

Fig.14 – Experimental results to view the system cooling behavior.

The system behavior for heating the chamber is presented in Fig.15. For these tests the bottom TEM was powered with 12 volts and the top TEM had its power supply voltage changed as shown in the same figure.

The traditional PID tuning method employed is based on firstly keeping only the proportional controlling part actuating, and then raising the proportional gain until the system starts to oscillate [15]. The proportional gain is then set at 80% of this value. Secondly, using the found proportional gain, the integral and derivative gains are obtained in a similar way.

Table I – Gains obtained by the trial method

Top TEM			
Gain	Kc	Ti	Tc
Value	20	17.625	2
Bottom TEM			
Gain	Kc	Ti	Tc
Value	49.9	9.8	0.664

A test with the chosen PID parameters with the set-point adjusted to 0ºC is shown in Fig.15, where the variation of the temperature as a function of the time is presented.

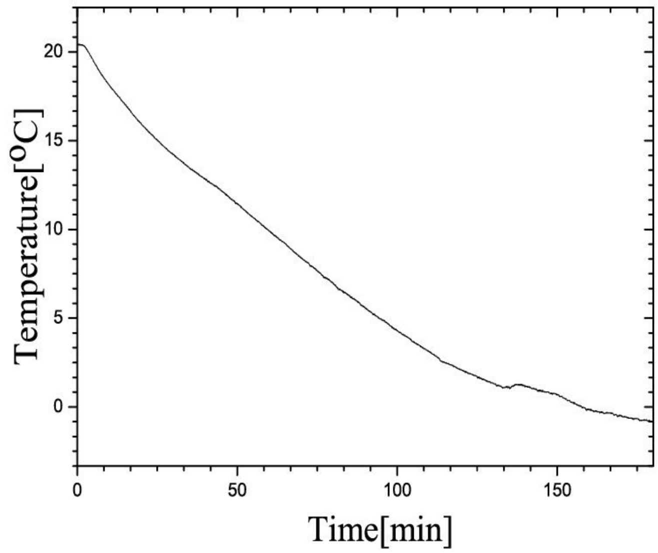

Fig.15 – Variation of temperature with time when the thermal chamber is set to 0ºC.

The thermal chamber takes approximately 180 minutes to reach -0.2ºC and no overshoot is found. An excellent temperature stability is observed, as seen in Fig.16. The gray lines are the temperature sensor measurements, which have a resolution of 0.03125ºC. It is important to notice that the maximum deviation is only around 0.16ºC. The black solid line shown is the result of the calculated average value using the 10 previous and 10 subsequent points at each instant of time.

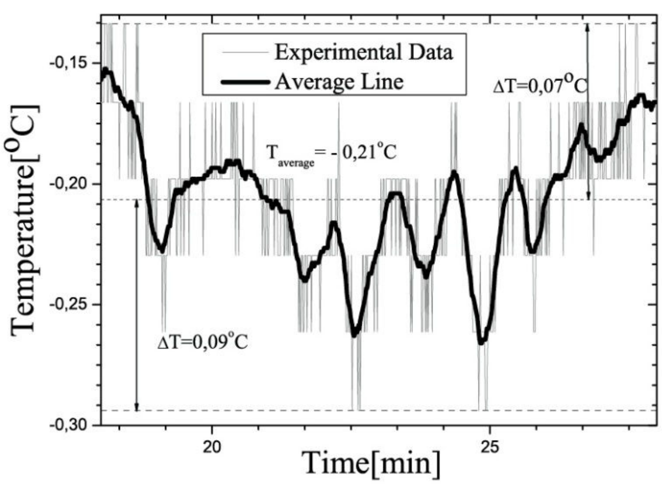

Fig.16 – Temperature variation near 0ºC.

The upper proposed temperature limit for the thermal chamber is 70ºC. A test with the set-point set to this value is shown in Fig.17. The response shows that a small overshoot (2ºC) is verified, but the stability is reached very quickly. In Fig.17 is possible to see how the middle temperature follows the internal temperature, as expected. Oscillations are also visible in the heat sink temperature, caused mainly by the air conditioning action in the room where the thermal chamber was tested.

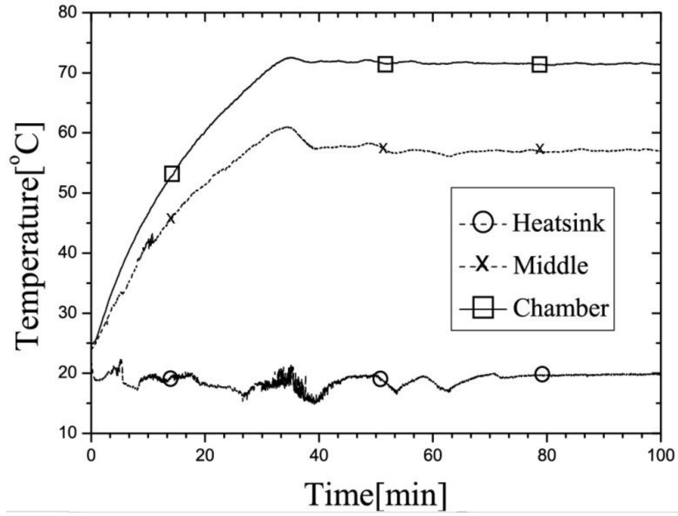

Fig.17 – System temperature graph for 70ºC set.

The temperature variation when the system is in steady state around 70ºC is similar to that observed for 0ºC. This variation is approximately 0.16ºC, as shown in Fig.18.

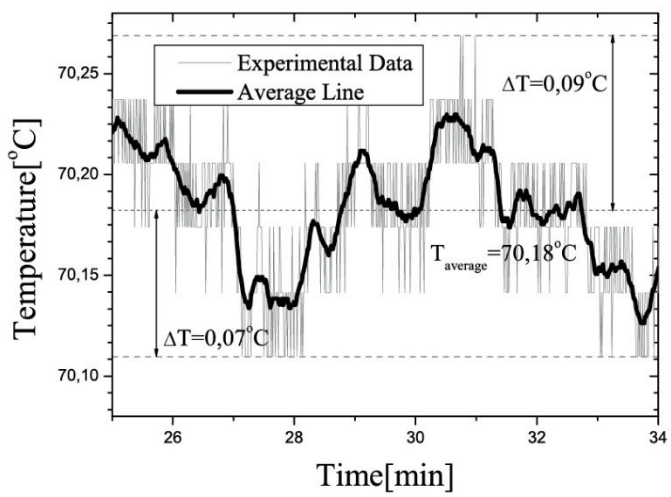

Fig.18 – Internal temperature variation at 70ºC.

In Fig.19 it is presented the transient response for various temperature set-points, showing that the system reaches its steady-state quickly when temperatures steps of 10ºC are applied.

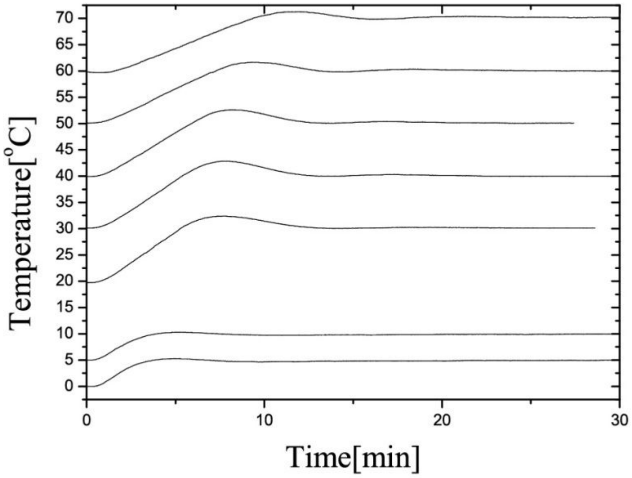

Fig.19 – Temperature response for various set-points.

Although the option of using two TEMs in series has been made to allow the thermal chamber to reach lowest temperatures, it was observed that this configuration also improves the system´s response to external disturbances. This can be seen in Fig.20, where it is observed that an external disturbance in the heat sink temperature (provoked by turning off the external fan) affects only the intermediate temperature, and does not affect the internal temperature of the thermal chamber.

In Fig.21 it is shown the behavior of the internal temperature when an external disturbance is forced.

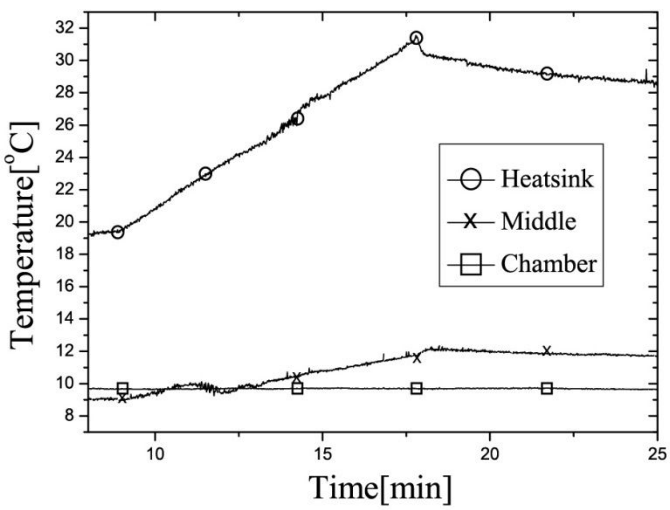

Fig.20 – System reaction to an external disturbance.

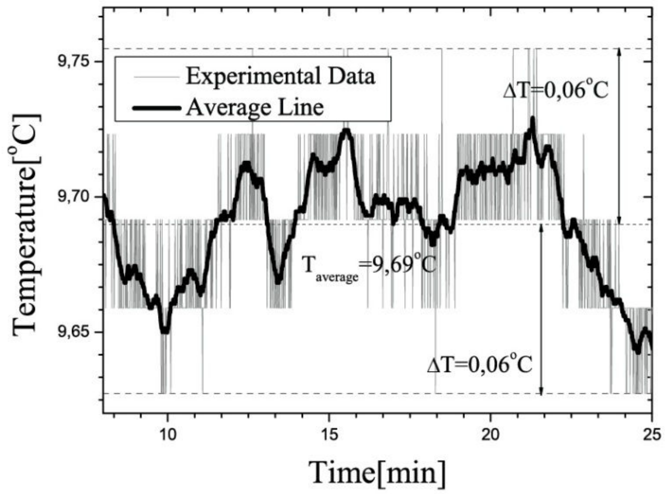

Fig.21 – Internal temperature oscillation when an external disturbance is forced.

In Fig.22 the behavior of the system when an external disturbance is provoked with the thermal chamber temperature around 50ºC is shown.

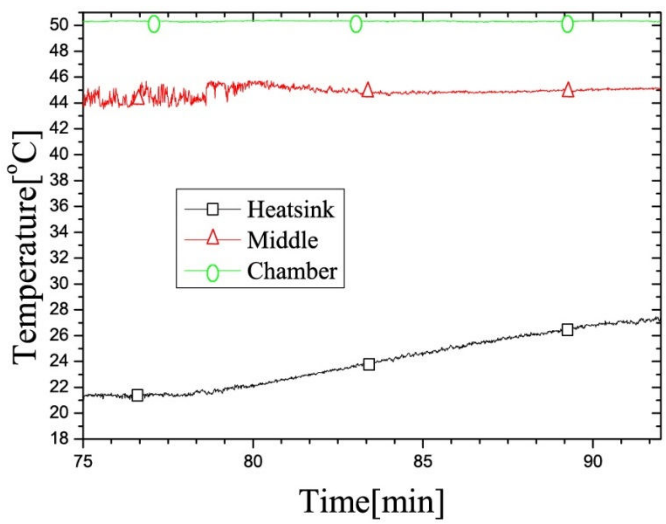

Fig.22 – System reaction to an external disturbance.

Observing the behavior of the thermal chamber temperature presented in Fig.23, is possible to notice that the system presents the same performance and the oscillation around the setpoint is not affected by the external disturbances.

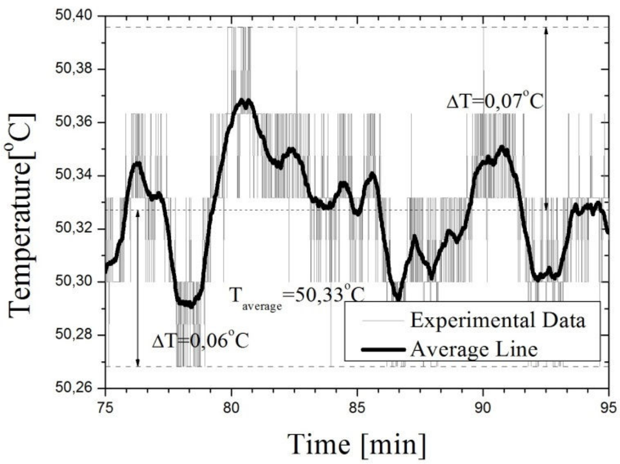

Fig.23 – Internal temperature oscillation when an external disturbance is forced.

VI. Conclusion

A low-cost, low-power and high performance table-top portable thermal chamber which covers the 0-70ºC temperature range was designed and fabricated, using a double TEM technique. Total power consumption at worst case scenario (when cooling) is only 175 W, which is very low when compared to the commercial available TEM thermal chambers [17], which present a power consumption usually greater than 350 W).

Due to its reduced volume and weight and the fact that it can be powered by two 12 V batteries, it can also be a valuable tool in field tests make possible field measurements.

The operation range of the thermal chamber is -5ºC to 70ºC, and an entrance for an inert gas like nitrogen allows the realization of tests below 0ºC without condensation.

The temperature fluctuation in steady state is only ±0.1ºC, and the relative temperature error to the set-point is ±0.2ºC, which outperforms most of the available commercial thermal chambers which are ten times more expensive.

References

[1] Laird Technologies, *A-Z Thermoelectric Design*. Available:http://www.lairdtech.com/Products/AZTec-Software-Download/[Accessed 20 November 2009]

[2] M. Page, *Akasa Nero AK-967 Heatsink Review*, 2009. Available:http//www.frosty-tech.com/articleview.cfm?articleID=2354[Accessed 5April 2010]

[3] Microchip Technology Inc., *PIC16F87XA Datasheet*. Available: http://ww1.microchip.com/downloads/en/DeviceDoc/39582b.pdf[Accessed 12March 2009]

[4] Analog Devices Inc., *Half-Duplex, iCoupler, Isolated RS-485 TransceiverADM2483 Datasheet*. Available: http://www.analog.com/static/importedfiles/data sheets/ADM2483.pdf [Accessed 12 March 2009]

[5] National Semiconductor Corp., *LM95071 Datasheet*. Available: http://www.national.com/ pf/LM/LM95071.html [Accessed 15 March 2009]

[6] Sensirion AG, *Datasheet SHT1X*. Available: http://www.sensirion.com/en/pdf/productinformation/Datasheet-humidity-sensor-SHT1x.pdf [Accessed 15 March 2009]

[7] Texas Instruments Inc., *TLV5616C, TLV5616I Datasheet*. Available:http://focus.ti.com/lit/ds/symlink/tlv5616.pdf [Accessed 12 March 2009]

[8] EPCOS, *NTC thermistors for temperature measurement Datasheet*. Available: http://www.epcos.com/inf/50/db/ntc09/Leaded-Disks B57891 M891.pdf [Accessed 15 March 2009]

[9] Analog Devices Inc., *2-Terminal IC Temperature TransducerAD590 Datasheet*. Available: http://www.analog.com/static/importedfiles/data sheets/AD590.pdf [Accessed 15 March 2009]

[10] C.C. Bradley, J. Chen and R.G. Huler, Instrumentation for the stable operation of laser diodes, *Rev. Sci. Instrum*. vol.61, no8, 1990, pp. 2097–2101.

[11] Shiuh-Jer Huang, Yi-Ho Lo, Metal Chamber Temperature control by Using Fuzzy PID Gain Auto-tuning strategy, *WSEAS Transactions on Systems and Control* vol.4, Jan 2009, pp. 1-10.

[12] Laird Technologies, *Ceramic Plate Series CP14,127,045Datasheet*. Available: http://www.lairdtech.com/WorkArea/linkit.aspx-?LinkIdentifier=id&ItemID=4291 [Accessed 13 March 2009]

[13] Avago Technologies, *HCPL-0452 0453 4502 4503 Datasheet*. Available:http://www.avagotech.com/docs/AV02-1392EN [Accessed 12 March 2009]

[14] Microchip Technology Inc., *TC4426 TC4427 TC4428 Datasheet*. Available:http://ww1.microchip.com/downloads/en/DeviceDoc/21422D.pdf [Accessed 22 March 2009]

[15] W.Y. Svrcek, D.P. Mahoney and B.R. Young, *A Real-Time Approach toProcess Control*, Wiley, West Sussex, 2006.

[16] E. Flaxer, Implementnf of a precision fast thermoelectric cooler controller using a personal computer parallel port connection and ADN8830controller, *Rev. Sci. Instrum*. vol.74, no8, 2003, pp. 3862–3873.

[17] Memmert. *Constant Climate Chamber HPP 108*. Avaible: http://www.memmert.com/fileadmin/template/memmert/pdfdata/HPP%20108_EN.pdf. [Acessed 2 August 2010]

[18] E.O. Virjoghe, D. Enescu, M. Ionel, and M.F. Stan. “Numerical simulation of Thermoelectric System,” in *Last Trends on Systems* vol.II, pp.630-635, July 2010.

[19] M. Lazard, “Heat Transfer in Thermoelectricity: Modeling, Optimization and Design”, in *Proc. 7th IASME/WSEAS Conf. Heat Transfer, Thermal Engineering and Environment*, Moscow, 2009, pp.129-134.

[20] N.Y.A. Shammas, S.Eio, and D. Chamund. “Semiconductor Devices and Their Use in Power Electronic Applications,” in *Proc 7th WSEAS Int. Conf Electric Power Syst, High Voltages, Electric Machines*, Venice, November 2007, pp 258-263.

[21] A.W. Spengler, E.C. Ferreira, and J.A. Siqueira Dias. “Precision Table-Top Portable Thermal Chamber with Double Thermoelectric Module,” in *Proc. 15th WSEAS Int. Conf. Circuits*, Corfy Island, July 2011, pp. 112-117.

[22] National Instruments, *National Instruments Labview*. Avaible:http://www.ni.com/labview/ [Acessed 02 December 2009].

Anderson W. Spengler was born in São Bento do Sul, SC, Brazil on March 9, 1986. He received the B.S. degree in physics (2008) and M.S. degree in electrical engineering (2010) from University of Campinas, UNICAMP, where he is currently working Ph.D. student. His research interests include electronic instrumentation, signal processing and fiber optics gyroscopes.

Elnatan C. Ferreira was born in Fortaleza, CE, Brazil on April 25, 1955. He received the B.S degree in physics from University of Ceara, CE, Brazil in 1981, and the M.S and the Ph.D. degrees in electrical engineering from University of Campinas, UNICAMP, respectively in 1984 and 1991. He joined the School of Electrical and Computer Engineering FEEC/UNICAMP as a Teaching Assistant in 1985, where he is currently an Associate Professor at the Department of Electronics and Microelectronics. His research interests include analog circuits and mixed-signal circuits, electronics instrumentation, signal processing and fiber optics sensors.

J. A. Siqueira Dias was born in Santos, SP, Brazil on October 15, 1954. He received the B.S, M.S. and Ph.D. degrees, all in electrical engineering, from the University of Campinas, UNICAMP, in 1979, 1982 and 1985, respectively. From 1980 to 1982 he was associated with the Laboratório de Eletrônica e Dispositivos – UNICAMP, working in the area of solid state device processing and semiconductor devices modeling. In 1983 he joined the School of Electrical and Computer Engineering – FEEC/UNICAMP, where he is currently the Vice-Head of the Department of Electronics and Microelectronics. His current research interests are in the areas of analog and mixed-signal integrated circuit design, electronics instrumentation and fiber optics sensors.